

Design optimization of vibration isolation system through minimization of vibration power flow

Shilin Xie[†], Siu Wing Or[‡] and Helen Lai Wa Chan^{††}

*Department of Applied Physics, The Hong Kong Polytechnic University,
Hung Hom, Kowloon, Hong Kong*

Ping Kong Choy^{††} and Peter Chou Kee Liu^{†††}

*ASM Assembly Automation Ltd., 3/F., Watson Centre, 16 Kung Yip Street,
Kwai Chung, New Territories, Hong Kong*

(Received January 12, 2007, Accepted February 13, 2008)

Abstract. A vibration power minimization model is developed, based on the mobility matrix method, for a vibration isolation system consisting of a vibrating source placed on an elastic support structure through multiple resilient mounts. This model is applied to investigate the design optimization of an X - Y motion stage-based vibration isolation system used in semiconductor wire-bonding equipment. By varying the stiffness coefficients of the resilient mounts while constraining the dynamic displacement amplitudes of the X - Y motion stage, the total power flow from the X - Y motion stage (the vibrating source) to the equipment table (the elastic support structure) is minimized at each frequency interval in the concerned frequency range for different stiffnesses of the equipment table. The results show that when the equipment table is relatively flexible, the optimal design based on the proposed vibration power minimization model gives significantly little power flow than that obtained using a conventional vibration force minimization model at some critical frequencies. When the equipment table is rigid enough, both models provide almost the same predictions on the total power flow.

Keywords: design optimization; elastic support structure; power flow; vibration isolation.

1. Introduction

Vibration isolation using multiple resilient mounts has received considerable attention in a broad domain of industrial fields, including those associated with the automobile, marine, aerospace, aeronautics, and automation industries. With the rapid development of computational technology in recent years, the design of vibration isolation systems through optimization techniques has become a promising approach for minimizing vibration transmission from vibrating sources to their isolated

[†] Research Associate

[‡] Assistant Professor, Corresponding author, E-mail: apswor@polyu.edu.hk

^{††} Chair Professor

^{†††} Technical Manager

^{††††} Chief Technical Officer

structures under some competitive constraints with minimal engineering efforts (Ashrafliuon 1993, Swanson *et al.* 1993, Snyman *et al.* 1995, Nayfeh *et al.* 1997, Leo *et al.* 1999, Tao *et al.* 2000, Yu *et al.* 2001, Ahn *et al.* 2003, Alkhatiba *et al.* 2004, Brake *et al.* 2005). Over the past decade, various design optimization methods have been developed or investigated for vibration isolation system applications. Some representative examples include gradient-based programming methods for isolating aircraft, marine, and automotive vehicle engines (Ashrafliuon 1993, Swanson *et al.* 1993, Snyman *et al.* 1995, Tao *et al.* 2001, Yu *et al.* 2001), genetic algorithms for designing passive linear suspensions (Alkhatiba *et al.* 2004) and optimizing vibration isolation of flex circuits in hard disk drives (Brake *et al.* 2005), nonlinear normal mode localization for optimizing vibration isolation systems with nonlinear isolators (Nayfeh *et al.* 1997), quadratic programming approach for designing active-passive vibration isolation systems (Leo *et al.* 1999), as well as artificial life algorithm for designing fluid mounts (Ahn *et al.* 2003). It should be noted that all the studies involving vibration isolation of vibrating sources from support structures solely considered rigid support structures, and the objective of design optimization problem was to minimize the total force transmitted from the vibrating sources to these rigid support structures.

Although the existing vibration force minimization models based on the assumption of rigid support structure generally yield reasonable predictions of what would observe in many real engineering situations, they may not be valid for some critical applications associated with the marine, aerospace, and automation equipment industries (Soliman and Hallam 1968, Ashrafliuon 1993, Choy and Wong 2004). For instance, highly accelerated motion stages (e.g., 20 m/s²) (i.e., the vibrating sources) are commonly installed on relatively flexible equipment tables (i.e., the support structures) via multiple resilient mounts to facilitate good vibration isolation performance during high-speed operation in semiconductor manufacturing equipment (e.g., wire-bonding and die-bonding equipment). It has been found experimentally that the vibrations transmitted from such motion stages generally excite their underneath equipment tables to exhibit noticeable elastic dynamics in the concerned frequency range (Choy and Wong 2004). This is different from the traditional vibration isolation system designs summarized in the previous paragraph, suggesting that the conventional vibration force minimization models may not be accurate enough to describe the vibration transmission behavior of such an isolation system.

By contrast, the power flow concept, which essentially combines the transmitted force and velocity responses into a single quantity (Goyder and White 1980, Pinnington 1987), provides a more complete description of vibration isolation systems equipped with elastic support structures as compared with the transmitted force or velocity response. For a multiple degree-of-freedom system having a number of multidirectional resilient mounts, the use of power flow concept has a great benefit to obtaining an insight into the mechanism of vibration transmission among system components (Koh and White 1996, Gardonio *et al.* 1997). Lee and Kim (2004) have demonstrated the capability of power flow technique to analyze the vibration and sound radiation levels of the compressor system mounted in the outdoor unit of an air conditioner. Moreover, it has been indicated that the minimization of power flow can be used as a cost function for active isolation design owing to its proven capability of providing optimal control results in comparison with other techniques (Gardonio *et al.* 1997). Therefore, it would be valuable to designers of vibration isolation systems to evaluate the system performance and improve the design if a vibration power minimization model tailored specifically to those systems with elastic support structures could be provided to substitute the conventional vibration force minimization models.

In this paper, we aim to develop a vibration power minimization model for the design of a

vibration isolation system comprising a vibrating source placed on an elastic support structure through multiple resilient mounts. First, the said model is derived using the mobility matrix method (Soliman and Hallam 1968, Gardonio *et al.* 1997). Second, the model is applied to a design case study involving the use of such an isolation system in industrial automatic wire-bonding equipment for semiconductor manufacturing. This characteristic type of vibration isolation system is formed by multiple resilient mounts situated between a highly accelerated X - Y motion stage and a comparatively flexible equipment table. The objective of design optimization is to minimize the total power flow to the equipment table through all resilient mounts. The stiffness coefficients of the resilient mounts are selected as the design variables with the upper and lower bounds. Constraints on the dynamic displacement amplitudes are imposed to the center of gravity (CG) of the X - Y motion stage. Sequential quadratic programming (SQP) algorithm (Schittkowski 1985, Fletcher 1987) is used to solve the design optimization problem. Third, the total power flow minimized using the developed model is investigated at each frequency interval in the concerned frequency range for different stiffnesses of equipment table, and the results are compared with those obtained using a conventional vibration force minimization model. Finally, some concluding remarks are provided.

2. Modeling of vibration isolation system with elastic support structure

2.1 Description of the vibration isolation system

Fig. 1 shows the vibration isolation system considered in the study. The rigid body represents the vibrating source. The resilient mounts are assumed to possess multidirectional elastic properties with hysteresis damping. The elastic panel that is simply supported on the floor is used to model the elastic support structure so as to take its naturally elastic dynamics into account. The rigid body mechanically couples with the elastic panel through N resilient mounts, and is subject to excitations during operations of the system. Two local coordinate systems, namely X - Y - Z and X_0 - Y_0 - Z_0 , are used to describe the motions of the isolation system. The origin of the local coordinate system X_0 - Y_0 - Z_0 is taken to coincide with the CG of the rigid body.

2.2 Equations of motion for the vibration isolation system

Fig. 2 illustrates the motion analysis scheme for the vibration isolation system in Fig. 1. The excitations due to the operations of the system are modeled as an external concentrated force vector

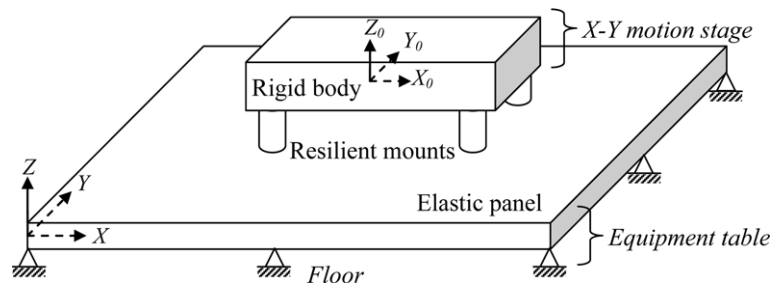


Fig. 1 Schematic diagram of the vibration isolation system

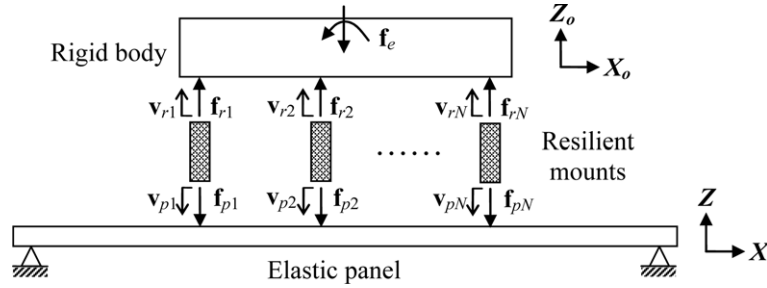


Fig. 2 The motion analysis scheme for the vibration isolation system shown in Fig. 1

(\mathbf{f}_e) applied directly to the CG of the rigid body, giving

$$\mathbf{f}_e = [F_x, F_y, F_z, M_x, M_y, M_z]^T \tag{1}$$

where F is the force, M is the moment, the subscripts x , y , and z represent the components of the variables in the x -, y -, and z -directions, respectively, and the superscript T denotes the transpose of a vector or a matrix.

All resilient mounts are vertically orientated and assumed to possess three-directional elastic properties with hysteresis damping. Thus, the force acting on each resilient mount junction is characterized by a force junction vector (\mathbf{f}) including three linear force components. For the i th resilient mount, the force junction vector associated with the rigid body-resilient mount junction and that associated with the elastic panel-resilient mount junction can be written, respectively, as

$$\mathbf{f}_{ri} = [F_{rxi}, F_{ryi}, F_{rzi}]^T \tag{2}$$

and

$$\mathbf{f}_{pi} = [F_{pxi}, F_{pyi}, F_{pzi}]^T \tag{3}$$

where the subscripts r and p represent the rigid body-resilient mount junction and the elastic panel-resilient mount junction, respectively. Similarly, the velocity at each resilient mount junction is characterized by a velocity junction vector (\mathbf{v}) grouped by three linear velocity components. The velocity junction vectors at the rigid body-resilient mount junction and the elastic panel-resilient mount junction are expressed, respectively, as

$$\mathbf{v}_{ri} = [\dot{u}_{ri}, \dot{v}_{ri}, \dot{w}_{ri}]^T \tag{4}$$

$$\mathbf{v}_{pi} = [\dot{u}_{pi}, \dot{v}_{pi}, \dot{w}_{pi}]^T \tag{5}$$

where \dot{u} , \dot{v} , and \dot{w} denote the linear velocities in the X_0 -, Y_0 -, and Z_0 -directions, respectively.

Grouping all rigid body-resilient mount junction force vectors into a single force junction vector and all rigid body-resilient mount junction velocity vectors into a single velocity junction vector, we have

$$\mathbf{f}_r = \begin{bmatrix} \mathbf{f}_{r1} \\ \mathbf{f}_{r2} \\ \vdots \\ \mathbf{f}_{rN} \end{bmatrix}, \quad \mathbf{v}_r = \begin{bmatrix} \mathbf{v}_{r1} \\ \mathbf{v}_{r2} \\ \vdots \\ \mathbf{v}_{rN} \end{bmatrix} \quad (6)$$

Similarly, for the elastic panel-resilient mount junctions, the single force and velocity junction vectors are as follows

$$\mathbf{f}_p = \begin{bmatrix} \mathbf{f}_{p1} \\ \mathbf{f}_{p2} \\ \vdots \\ \mathbf{f}_{pN} \end{bmatrix}, \quad \mathbf{v}_p = \begin{bmatrix} \mathbf{v}_{p1} \\ \mathbf{v}_{p2} \\ \vdots \\ \mathbf{v}_{pN} \end{bmatrix} \quad (7)$$

Using the mobility matrix method (Soliman and Hallam 1968, Gardonio *et al.* 1997), the dynamics of the rigid body can be described by the following mobility equation

$$\mathbf{v}_r = \mathbf{M}_{r1} \mathbf{f}_r + \mathbf{M}_{r2} \mathbf{f}_e \quad (8)$$

where \mathbf{M}_{r1} and \mathbf{M}_{r2} are the mobility matrices of the rigid body associated with the rigid body-resilient mount junction force vector \mathbf{f}_r and the external concentrated force vector \mathbf{f}_e , respectively.

For harmonic excitations of the form $e^{j\omega t}$, the six degree-of-freedom motion equation of the rigid body in the local coordinate system X_0 - Y_0 - Z_0 can be expressed in terms of the velocities of its CG at a single frequency ω as follows (Harris 2002)

$$j\omega \mathbf{M}_c \mathbf{v}_c = \sum_{i=1}^N \mathbf{R}_i \mathbf{f}_i + \mathbf{f}_e \quad (9)$$

$$\mathbf{M}_c = \text{diag}(m, m, m, I_{xx}, I_{yy}, I_{zz}) \quad (10)$$

$$\mathbf{v}_c = [\dot{u}_c, \dot{v}_c, \dot{w}_c, \dot{\theta}_{cx}, \dot{\theta}_{cy}, \dot{\theta}_{cz}]^T \quad (11)$$

$$\mathbf{R}_i = \begin{bmatrix} 1 & 0 & 0 \\ 0 & 1 & 0 \\ 0 & 0 & 1 \\ 0 & -z_{0i} & y_{0i} \\ z_{0i} & 0 & -x_{0i} \\ -y_{0i} & x_{0i} & 0 \end{bmatrix} \quad (12)$$

where \mathbf{M}_c is the mass matrix of the rigid body, \mathbf{v}_c is the velocity vector of the CG of the rigid body, \mathbf{R}_i is the location matrix of force acting on the rigid body by the i th mount, m is the mass of the rigid body, I_{xx} , I_{yy} , and I_{zz} are the moments of inertia of the rigid body with respect to the X_0 -, Y_0 -, and Z_0 -axes, respectively, and x_{0i} , y_{0i} , and z_{0i} are the position coordinates of the i th rigid body-resilient mount junction in the local coordinate system X_0 - Y_0 - Z_0 . Combining Eqs. (6) and (9), we have

$$j\omega \mathbf{M}_c \mathbf{v}_c = \mathbf{R} \mathbf{f}_r + \mathbf{f}_e \quad (13)$$

$$\mathbf{R} = [\mathbf{R}_1 \ \mathbf{R}_2 \ \dots \ \mathbf{R}_N] \tag{14}$$

It is known that the rigid body-resilient mount junction velocity vector \mathbf{v}_r is related to the velocity vector \mathbf{v}_c of the CG of the rigid body by Harris (2002)

$$\mathbf{v}_r = \mathbf{R}^T \mathbf{v}_c \tag{15}$$

where \mathbf{R}^T is the transpose of \mathbf{R} . Substituting Eq. (15) into Eq. (13), the mobility matrices of the rigid body in Eq. (8) can be expressed as

$$\mathbf{M}_{r1} = (1/j\omega)\mathbf{R}^T\mathbf{M}_c^{-1}\mathbf{R} \tag{16}$$

$$\mathbf{M}_{r2} = (1/j\omega)\mathbf{R}^T\mathbf{M}_c^{-1} \tag{17}$$

To facilitate description of the dynamics of the elastic panel, a local coordinate system X - Y - Z is used as shown in Fig. 1. Accordingly, the mobility equation of the elastic panel in the local coordinate system X - Y - Z can be expressed as

$$\mathbf{v}_p = \mathbf{M}_p \mathbf{f}_p \tag{18}$$

$$\mathbf{M}_p = \begin{bmatrix} \mathbf{m}_{p11} & \mathbf{m}_{p12} & \dots & \mathbf{m}_{p1N} \\ \mathbf{m}_{p21} & \mathbf{m}_{p22} & \dots & \mathbf{m}_{p2N} \\ \vdots & \vdots & \vdots & \vdots \\ \mathbf{m}_{pN1} & \mathbf{m}_{pN2} & \dots & \mathbf{m}_{pNN} \end{bmatrix} \tag{19}$$

where \mathbf{M}_p is the mobility matrix of the elastic panel. It is noted from Eq. (19) that the diagonal element \mathbf{m}_{pii} is the point mobility matrix at the i th elastic panel-resilient mount junction, while the non-diagonal element \mathbf{m}_{pik} is the transfer mobility matrix between the i th elastic panel-resilient mount junction (i.e., the response point) and the k th elastic panel-resilient mount junction (i.e., the excitation point). \mathbf{m}_{pik} in Eq. (19) can further be expressed as

$$\mathbf{m}_{pik} = \begin{bmatrix} m_{pik}^{\dot{u}Fx} & m_{pik}^{\dot{u}Fy} & m_{pik}^{\dot{u}Fz} \\ m_{pik}^{\dot{v}Fx} & m_{pik}^{\dot{v}Fy} & m_{pik}^{\dot{v}Fz} \\ m_{pik}^{\dot{w}Fx} & m_{pik}^{\dot{w}Fy} & m_{pik}^{\dot{w}Fz} \end{bmatrix} \quad (i = 1, \dots, N; k = 1, \dots, N) \tag{20}$$

Generally, the flexural wave motion is more important than the in-plane shear and longitudinal wave motions in the vibroacoustic and power flow analyses of plate-like structures (Koh and White 1996, Gardonio *et al.* 1997). Hence, the contributions of the two horizontal components of each elastic panel-resilient mount junction force vector are only modeled as the concentrated moments about the X - and Y -axes due to the thickness of the elastic panel for the dynamic analysis of the elastic panel. Consequently, the following relationships among the three components of the i th elastic panel-resilient mount junction velocity vector hold valid

$$\dot{u}_{pi} = -\frac{h}{2} \frac{\partial \dot{w}_{pi}}{\partial x} \tag{21}$$

$$\dot{v}_{pi} = -\frac{h}{2} \frac{\partial \dot{w}_{pi}}{\partial y} \quad (22)$$

where h is the thickness of the elastic panel.

Using Eqs. (21) and (22), and according to the mobility formula of finite panel (Cremer *et al.* 1988), the elements in \mathbf{m}_{pik} (Eq. (20)) for an elastic panel with the simply supported boundary condition can be expressed as

$$m_{pik}^{\dot{u}Fx} = \frac{j\omega h^2}{4} \sum_{m=1}^{\infty} \sum_{n=1}^{\infty} \frac{\psi_{m,n}^{(x)}(x_i, y_i) \psi_{m,n}^{(x)}(x_k, y_k)}{\Lambda[\omega_{m,n}^2(1+j\eta_p) - \omega^2]} \quad (23a)$$

$$m_{pik}^{\dot{u}Fy} = -\frac{j\omega h^2}{4} \sum_{m=1}^{\infty} \sum_{n=1}^{\infty} \frac{\psi_{m,n}^{(x)}(x_i, y_i) \psi_{m,n}^{(y)}(x_k, y_k)}{\Lambda[\omega_{m,n}^2(1+j\eta_p) - \omega^2]} \quad (23b)$$

$$m_{pik}^{\dot{u}Fz} = \frac{j\omega h}{2} \sum_{m=1}^{\infty} \sum_{n=1}^{\infty} \frac{\psi_{m,n}^{(x)}(x_i, y_i) \varphi_{m,n}(x_k, y_k)}{\Lambda[\omega_{m,n}^2(1+j\eta_p) - \omega^2]} \quad (23c)$$

$$m_{pik}^{\dot{v}Fx} = -\frac{j\omega h^2}{4} \sum_{m=1}^{\infty} \sum_{n=1}^{\infty} \frac{\psi_{m,n}^{(y)}(x_i, y_i) \psi_{m,n}^{(x)}(x_k, y_k)}{\Lambda[\omega_{m,n}^2(1+j\eta_p) - \omega^2]} \quad (23d)$$

$$m_{pik}^{\dot{v}Fy} = \frac{j\omega h^2}{4} \sum_{m=1}^{\infty} \sum_{n=1}^{\infty} \frac{\psi_{m,n}^{(y)}(x_i, y_i) \psi_{m,n}^{(y)}(x_k, y_k)}{\Lambda[\omega_{m,n}^2(1+j\eta_p) - \omega^2]} \quad (23e)$$

$$m_{pik}^{\dot{v}Fz} = -\frac{j\omega h}{2} \sum_{m=1}^{\infty} \sum_{n=1}^{\infty} \frac{\psi_{m,n}^{(y)}(x_i, y_i) \varphi_{m,n}(x_k, y_k)}{\Lambda[\omega_{m,n}^2(1+j\eta_p) - \omega^2]} \quad (23f)$$

$$m_{pik}^{\dot{w}Fx} = \frac{j\omega h}{2} \sum_{m=1}^{\infty} \sum_{n=1}^{\infty} \frac{\varphi_{m,n}(x_i, y_i) \psi_{m,n}^{(x)}(x_k, y_k)}{\Lambda[\omega_{m,n}^2(1+j\eta_p) - \omega^2]} \quad (23g)$$

$$m_{pik}^{\dot{w}Fy} = -\frac{j\omega h}{2} \sum_{m=1}^{\infty} \sum_{n=1}^{\infty} \frac{\varphi_{m,n}(x_i, y_i) \psi_{m,n}^{(y)}(x_k, y_k)}{\Lambda[\omega_{m,n}^2(1+j\eta_p) - \omega^2]} \quad (23h)$$

$$m_{pik}^{\dot{w}Fz} = j\omega \sum_{m=1}^{\infty} \sum_{n=1}^{\infty} \frac{\varphi_{m,n}(x_i, y_i) \varphi_{m,n}(x_k, y_k)}{\Lambda[\omega_{m,n}^2(1+j\eta_p) - \omega^2]} \quad (23i)$$

where $\omega_{m,n}$ and $\varphi_{m,n}$ are the (m, n) th natural frequency and modal shape function of the elastic panel, respectively; $\psi_{m,n}^{(x)}$ and $\psi_{m,n}^{(y)}$ are the partial differentials of $\varphi_{m,n}$ with respect to x and y , respectively; Λ and η_p are the modal mass and the loss factor of the elastic panel, respectively; and (x_i, y_i) and (x_k, y_k) are the location coordinates of the i th and the k th elastic panel-resilient mount junction in the local coordinate system X - Y - Z , respectively. Λ , $\omega_{m,n}$, $\varphi_{m,n}$, $\psi_{m,n}^{(x)}$, and $\psi_{m,n}^{(y)}$ can further be written as follows

$$\Lambda = \frac{\rho abh}{4}, \quad \omega_{m,n} = \left[\left(\frac{m\pi}{a} \right)^2 + \left(\frac{n\pi}{b} \right)^2 \right] \sqrt{\frac{D_0}{\rho h}} \quad (24a)$$

$$\varphi_{m,n}(x, y) = \sin \frac{m\pi x}{a} \sin \frac{n\pi y}{b} \quad (24b)$$

$$\psi_{m,n}^{(x)}(x,y) = -\frac{m\pi}{a}\cos\frac{m\pi x}{a}\sin\frac{n\pi y}{b} \tag{24c}$$

$$\psi_{m,n}^{(y)}(x,y) = \frac{n\pi}{b}\sin\frac{m\pi x}{a}\cos\frac{n\pi y}{b} \tag{24d}$$

where a and b are the dimensions of the elastic panel in the X - and Y -directions, respectively; $D_0 = Eh^3/12(1-\mu^2)$ is the flexural rigidity of the elastic panel; and ρ , E , and μ are the mass density, Young’s modulus, and Poisson’s ratio of the elastic panel, respectively.

For the i th resilient mount, the rigid body-resilient mount junction force \mathbf{f}_i is related to the velocity at the rigid body-resilient mount junction \mathbf{v}_i and that at the elastic panel-resilient mount junction \mathbf{v}_p by

$$\mathbf{f}_i = -(1/j\omega)\mathbf{K}_{mi}[\mathbf{v}_i - \mathbf{v}_p] \tag{25}$$

$$\mathbf{K}_{mi} = (1 + j\eta_{mi})\text{diag}(k_{mxi}, k_{myi}, k_{mzi}) \tag{26}$$

where the subscript m represents the resilient mount; \mathbf{K}_{mi} is the complex stiffness coefficient matrix of the i th resilient mount; k_{mxi} , k_{myi} , and k_{mzi} are the stiffness coefficients of the i th resilient mount in the X -, Y -, and Z -directions, respectively; and η_{mi} is the loss factor of the i th resilient mount. Utilizing Eqs. (6) and (7), Eq. (25) can be rewritten as

$$\mathbf{f}_r = -(1/j\omega)\mathbf{K}_m[\mathbf{v}_r - \mathbf{v}_p] \tag{27}$$

$$\mathbf{K}_m = \begin{bmatrix} \mathbf{K}_{m1} & & & \\ & \mathbf{K}_{m2} & & \\ & & \ddots & \\ & & & \mathbf{K}_{mN} \end{bmatrix} \tag{28}$$

According to the force equilibrium principle, the following relationship between the rigid body-resilient mount junction force \mathbf{f}_r and the elastic panel-resilient mount junction force \mathbf{f}_p holds true

$$\mathbf{f}_p = -\mathbf{f}_r \tag{29}$$

Combining Eqs. (8), (18), (27), and (29), the elastic panel-resilient mount junction velocity vector can be formulated as

$$\mathbf{v}_p = (\mathbf{Z}_m + \mathbf{M}_p^{-1} + \mathbf{Z}_m\mathbf{M}_r\mathbf{M}_p^{-1})^{-1}\mathbf{Z}_m\mathbf{M}_r\mathbf{f}_e \tag{30}$$

$$\mathbf{Z}_m = (1/j\omega)\mathbf{K}_m \tag{31}$$

From Eqs. (18) and (30), the elastic panel-resilient mount junction force vector \mathbf{f}_p can be solved. Then, the total time-averaged power flow from N resilient mounts to the elastic panel can be expressed as (Goyder and White 1980)

$$P_t = -\frac{1}{2}\text{Re}\{\mathbf{f}_p^H\mathbf{v}_p\} \tag{32}$$

where the superscript H denotes the transpose and conjugate of a matrix or vector.

3. Statement of vibration power minimization design problem

A design optimization problem, which comprises an objective function and a set of constraints and/or bounds, can be expressed mathematically as

$$\min J(\mathbf{k}), \quad \mathbf{k} \in R^{nv} \tag{33a}$$

subject to

$$c_i(\mathbf{k}) \leq 0 \quad i = 1, \dots, nc \tag{33b}$$

$$\mathbf{k}_l \leq \mathbf{k} \leq \mathbf{k}_u \tag{33c}$$

where $J(\mathbf{k})$ is the objective function to be minimized, \mathbf{k} is the vector including nv design variables, $c_i(\mathbf{k})$ represents the i th equality/inequality constraint, nc is the total number of constraints, and \mathbf{k}_u and \mathbf{k}_l are the upper and lower bounds of the design variables, respectively.

In the design optimization of the vibration isolation system shown in Fig. 1, the total power flow from the rigid body to the elastic panel is considered as the objective function to be minimized, whereas the three-directional stiffness coefficients of the resilient mounts are chosen as the design variables. The upper and lower bounds of the three-directional stiffness coefficients of the resilient mounts are imposed to the design optimization problem of the isolation system for obtaining a reasonable solution. The lower bound of the stiffness coefficients is determined by the maximum static loading capability of the resilient mounts. The upper bound of the stiffness coefficients is also set to avoid the probable wave effects induced by the exorbitant “stiff” mount (Swanson *et al.* 1993). To ensure a certain level of motion accuracy during operations of the isolation system, the movement of the rigid body (i.e., the vibrating machine) is also limited and can be expressed as the constraints on the dynamic displacement amplitudes of its CG, giving

$$|\mathbf{d}_c| \leq \mathbf{d}_{\max} \tag{34}$$

$$\mathbf{d}_c = [u_c, v_c, w_c, \theta_{cx}, \theta_{cy}, \theta_{cz}]^T \tag{35}$$

where \mathbf{d}_{\max} is the maximum allowable dynamic displacement amplitude and \mathbf{d}_c is the dynamic displacement vector of the CG of the rigid body.

Therefore, the design optimization problem can be written as

$$\min_{\mathbf{k}_{mi} (i=1, \dots, N)} P_t \tag{36a}$$

subject to

$$|\mathbf{d}_c| \leq \mathbf{d}_{\max} \tag{36b}$$

$$\mathbf{k}_{li} \leq \mathbf{k}_{mi} \leq \mathbf{k}_{ui} \tag{36c}$$

The above equations give a nonlinear constrained design optimization problem. It is known that sequential quadratic programming (SQP) algorithm may be the most preferable solver for nonlinear constrained optimization problem compared to other solvers in terms of efficiency, accuracy, and

percentage of successful solutions (Schittkowski 1985). The solution of the Kuhn-Tucker (KT) equations forms the basis of SQP algorithm. In SQP, a quadratic programming (QP) sub-problem generated through approximating the Hessian matrix of the Lagrangian function with a quasi-Newton updating method is solved in each major iteration (Fletcher 1987). In this study, SQP algorithm is used to solve the nonlinear constrained optimization problem given by Eq. (36).

4. Design case study

4.1 Application background

In this section, the vibration power minimization model developed in Sections 2 and 3 is applied to the design optimization of an X - Y motion stage-based vibration isolation system used in ASM wire-bonding equipment. The wire-bonding equipment is one of the most important types of automation equipment for semiconductor manufacturing. To facilitate a standard operational cycle for bonding a metallic wire between a first bonding site typically on an integrated circuit (IC) and a second bonding site typically on a substrate, it is necessary for the moving part of the X - Y motion stage to perform a 2 mm translation from the first bonding site to the second bonding site within 30 ms (Choy and Wong 2004). This requires acceleration as high as 20 m/s^2 that, in turn, results in large dynamic forces transmitted from the X - Y motion stage to the equipment table due to the effect of inertia. This highly accelerated X - Y motion stage needs to be installed on a relatively flexible equipment table via multiple resilient mounts so as to mitigate vibration transmission during high-speed operations. Therefore, design optimization of this type of vibration isolation system is technologically important. The proposed vibration power minimization model may be more appropriate in comparison with the conventional vibration force minimization models.

4.2 Optimization solution method

Referring to Fig. 1, the X - Y motion stage (modeled as the rigid body) is installed in the middle of the equipment table (modeled as the elastic panel) through multiple resilient mounts (modeled using four identical resilient mounts). Table 1 shows the geometric and material parameters of such a specific vibration isolation system. The X - Y motion stage is assumed to be a rectangular block made of stainless steel. The equipment table is treated as a rectangular plate made of aluminum alloy

Table 1 Geometric and material parameters of the X - Y motion stage-based vibration isolation system

System components	Geometric parameters			Material parameters		
Rigid body (X - Y motion stage)	Length	a_r	500 mm	Density	ρ_r	7800 kg/m ³
	Width	b_r	200 mm			
	Height	h_r	100 mm			
Elastic panel (Equipment table)	Length	a	1200 mm	Young's modulus	E	71 GPa
	Width	b	1000 mm	Density	ρ_p	2700 kg/m ³
	Thickness	h	5 mm	Poisson's ratio	μ	0.3
Resilient mounts				Loss factor	η_p	0.005
				Loss factor	η_m	0.05

Table 2 Position coordinates of the resilient mount junctions

Resilient mount number	Position coordinates (mm)					
	x_{0i}	y_{0i}	z_{0i}	x_i	y_i	z_i
$i = 1$	-250	-100	-50	350	400	25
$i = 2$	250	-100	-50	850	400	25
$i = 3$	250	100	-50	850	600	25
$i = 4$	-250	100	-50	350	600	25

7075. Table 2 gives the position coordinates of each resilient mount junction. Based on the application background described in the previous paragraph, and according to the experimental modal analysis results performed by Choy and Wong (2004) in ASM, a representative motion status of the moving part, i.e., a translational motion of the moving part in the x - y direction, is selected as a specific case in this study. This case leads to $\mathbf{F} = [280 \text{ N}, 160 \text{ N}, 500 \text{ N}, -16 \text{ Nm}, 14 \text{ Nm}, 0 \text{ Nm}]^T$, which denotes force excitations in the x -, y -, and z -directions and moment excitations about the x - and y -axes. Besides, the frequency range of interest for the design optimization is [1, 200] Hz as the elastic dynamics of the equipment table is commonly pronounced in this frequency range (Choy and Wong 2004).

The upper and lower bounds of the three-directional stiffness coefficients of each resilient mount are known to be

$$50(\text{kN/m}) \leq (k_{mx}, k_{my}, k_{mz}) \leq 1000(\text{kN/m}) \tag{37}$$

and the constraints on the dynamic displacement amplitudes of the CG of the X - Y motion stage are

$$|u_c| \leq 2 \text{ mm}, \quad |v_c| \leq 2 \text{ mm} \tag{38}$$

In order to reduce the errors induced by the truncated modes of the equipment table, the first 68 modes of the equipment table, as tabulated in Table 3, were used in the analysis with the highest modal frequency near 1000 Hz.

The design optimization problem (Eq. (36)) was then solved by assuming one excitation frequency at a time starting from 1 to 200 Hz. This led to a total of 200 optimization problems to be solved. It is known from Eq. (32) that the objective function is not continuously differentiable. Hence, the solution of each optimization problem obtained using SQP algorithm depends on the starting point of design variables and may not be globally minimized. To obtain the global minimum of each optimization problem at the maximum probability, multiple equidistant starting points of design variables (39 in total) in the stiffness range of 50-1000 kN/m were used in each optimization problem. The solution corresponding to the minimum of the objective function values obtained from these different starting points was then regarded as the “global” optimal solution of an optimization problem.

In the present study, a conventional vibration force minimization model was also examined with the same constraints and optimization solution method so as to provide a fair comparison with the proposed vibration power minimization model. In the conventional vibration force minimization model, the support structure (the equipment table in the current design case study) is treated as a rigid panel rather than an elastic panel, and the total force transmitted to such a rigid panel is

Table 3 Modal frequencies of the equipment table

Order	<i>m</i>	<i>n</i>	$\omega_{m,n}/2\pi$ (Hz)	Order	<i>m</i>	<i>n</i>	$\omega_{m,n}/2\pi$ (Hz)	Order	<i>m</i>	<i>n</i>	$\omega_{m,n}/2\pi$ (Hz)
1	1	1	20.65	25	5	4	406.60	49	9	2	734.32
2	2	1	46.04	26	6	3	414.39	50	8	4	736.69
3	1	2	57.22	27	7	1	426.91	51	6	6	743.46
4	2	2	82.61	28	4	5	440.12	52	1	8	788.48
5	3	1	88.36	29	1	6	447.23	53	9	3	795.25
6	1	3	118.15	30	7	2	463.48	54	5	7	808.80
7	3	2	124.93	31	2	6	472.62	55	2	8	813.88
8	2	3	143.55	32	6	4	499.70	56	8	5	846.38
9	4	1	147.61	33	3	6	514.94	57	7	6	853.49
10	4	2	184.17	34	5	5	516.29	58	3	8	856.19
11	3	3	185.86	35	7	3	524.41	59	10	1	858.56
12	1	4	203.47	36	8	1	553.87	60	9	4	880.57
13	5	1	223.78	37	4	6	574.18	61	10	2	895.13
14	2	4	228.86	38	8	2	590.43	62	6	7	901.90
15	4	3	245.11	39	1	7	605.67	63	4	8	915.44
16	5	2	260.35	40	6	5	609.39	64	10	3	956.07
17	3	4	271.18	41	7	4	609.73	65	8	6	980.44
18	1	5	313.16	42	2	7	631.06	66	9	5	990.26
19	6	1	316.88	43	5	6	650.36	67	5	8	991.61
20	5	3	321.28	44	8	3	651.37	68	1	9	995.68
21	4	4	330.43	45	3	7	673.38				
22	2	5	338.55	46	9	1	697.75				
23	6	2	353.45	47	7	5	719.42				
24	3	5	380.87	48	4	7	732.62				

minimized. The corresponding design problem is as follows

$$\min_{\mathbf{k}_{m\hat{p}} (i=1, \dots, N)} F_t \quad (38a)$$

subject to

$$|\mathbf{d}_c| \leq \mathbf{d}_{\max} \quad (38b)$$

$$\mathbf{k}_{li} \leq \mathbf{k}_{mi} \leq \mathbf{k}_{ui} \quad (38c)$$

where $F_t = \sum_{i=1}^N (\bar{\mathbf{f}}_{pi}^T \bar{\mathbf{f}}_{pi})^{1/2}$ is the total transmitted force and $\bar{\mathbf{f}}_{pi}$ is the *i*th rigid panel-resilient mount junction force vector.

5. Results and discussion

Fig. 3 shows the frequency dependence of the total power flow to the equipment table obtained from the proposed vibration power minimization model (Eq. (36)) and the conventional vibration force minimization model (Eq. (38)). It is clear that the total power flow can be significantly

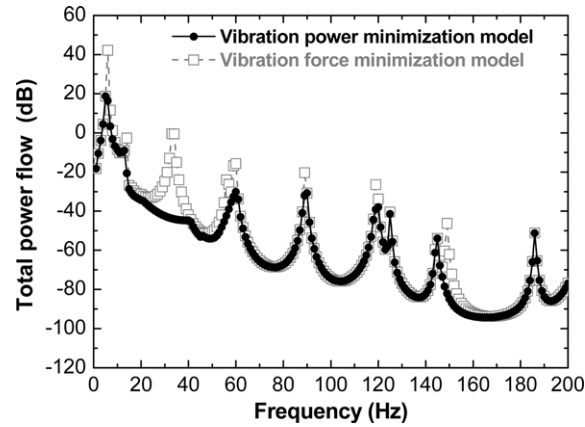


Fig. 3 Frequency dependence of the total power flow to the equipment table obtained from the proposed vibration power minimization model and the conventional vibration force minimization model

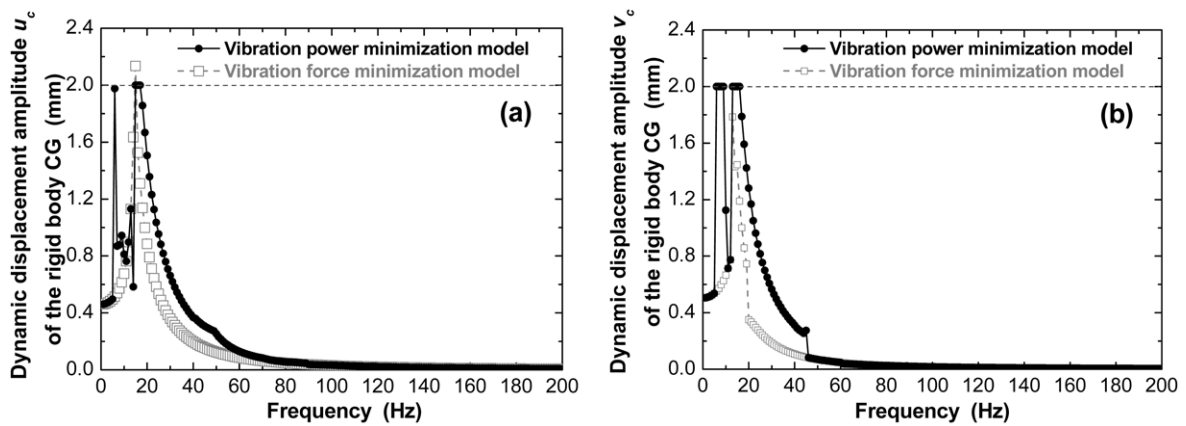


Fig. 4 Comparisons of the dynamic displacement amplitudes (a) u_c and (b) v_c of the CG of the X - Y motion stage obtained from the proposed vibration power minimization model and the conventional vibration force minimization model. The horizontal lines show the constraints imposed on u_c and v_c

reduced in the frequency ranges of 5-9, 13-41, 52-61, 88-90, 118-121, and 148-166 Hz by employing the proposed vibration power minimization model. Specifically, the maximum reduction in the total power flow is as large as 43 dB at 34 Hz. The observation indicates that the elastic dynamic characteristics of the equipment table have a crucial effect on the design optimization of the vibration isolation system at these frequencies. The smaller differences in the total power flow at other frequencies suggest that the elasticity of the equipment table merely exerts a slight influence on the design optimization. Nevertheless, the proposed vibration power minimization model provides a comparatively better “optimized” design for the vibration isolation system equipped with a relatively flexible equipment table. Fig. 4 illustrates the comparisons of the dynamic displacement amplitudes u_c and v_c of the CG of the X - Y motion stage obtained from the proposed and conventional vibration minimization models. It is found that the constraints on the dynamic displacement amplitudes of the CG of the X - Y motion stage are active in the first two frequency ranges of 5-9 and 13-41 Hz. The differences in the results predicted by the two vibration

minimization models are also noticeable in these two frequency ranges. In more details, the proposed vibration power minimization model gives larger u_c (Fig. 4(a)) and v_c (Fig. 4(b)) in the first two frequency ranges of 5-9 and 13-41 Hz compared to the conventional vibration force minimization model except that u_c of the conventional vibration force minimization model is greatly enhanced and even overpasses the preset constraint of ≤ 2 mm (Eq. (38)) at 15 Hz. At elevated frequencies of >60 Hz, both models give almost the same predictions of u_c and v_c as expected.

In fact, the developed vibration power minimization model is based on the assumption of an elastic support structure, while the conventional vibration force minimization model assumes a rigid support structure. When the equipment table is relatively flexible, there exist significant differences in the total power flow between the two vibration minimization models, as evidenced in Fig. 3. In order to further examine the effects of the dynamic characteristics of the equipment table on the application potential of these two vibration minimization models, two additional case studies were also performed by varying the stiffness of the equipment table. In the first case we increased the stiffness of the equipment table by 10 times, and in the second case we further increased the stiffness by 100 times. The first 46 modes of the equipment table, with the highest modal frequency near 2000 Hz, were used in the first case. For the second case, the first 15 modes of the equipment table with the highest modal frequency near 2500 Hz were considered. The design results are shown in Figs. 5 and 6 and Figs. 7 and 8 for the first and second cases, respectively.

Fig. 5 shows the comparison of the total power flow to the equipment table between the proposed vibration power minimization model and the conventional vibration force minimization model after an increase of 10 times in the table stiffness. Compared to Fig. 3, it is seen that when a relatively stiff equipment table is used, the total power flow that can be minimized by the proposed vibration power minimization model becomes less significant. While the minimization effect is still obvious in the frequency ranges of 12-15, 66-75, and 146-152 Hz, the maximum reduction in the total power flow is only 33 dB at 71 Hz (compared to 43 dB at 34 Hz in Fig. 3). The reason may be explained by the increase in table stiffness, which reduces the number of modes of the equipment table allowed in the 200 Hz frequency range. Consequently, the effects of elastic dynamics of the equipment table on the design optimization of the vibration isolation system are weakened. From

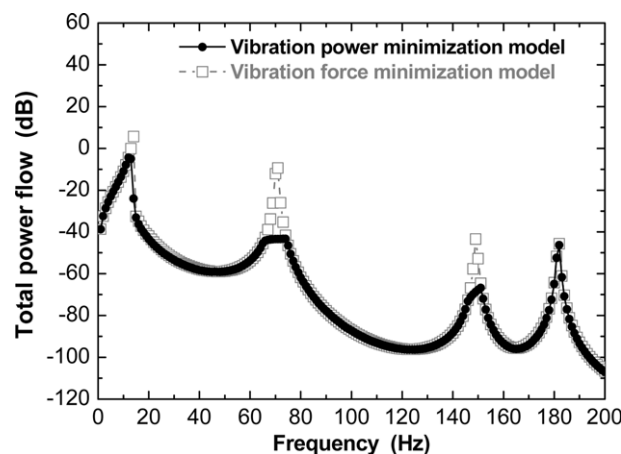


Fig. 5 Frequency dependence of the total power flow to the equipment table obtained from the proposed vibration power minimization model and the conventional vibration force minimization model after an increase of 10 times in the stiffness of the equipment table

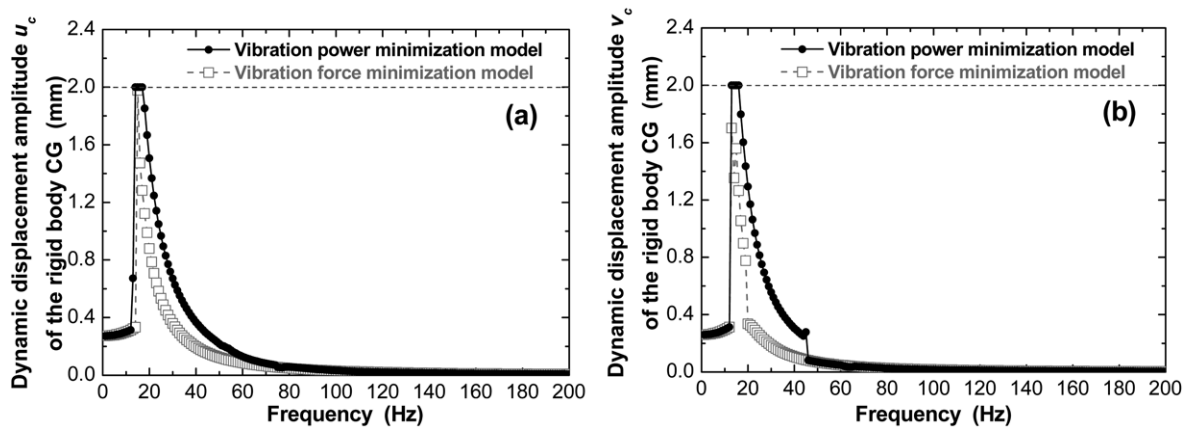


Fig. 6 Comparisons of the dynamic displacement amplitudes (a) u_c and (b) v_c of the CG of the X-Y motion stage obtained from the proposed vibration power minimization model and the conventional vibration force minimization model after an increase of 10 times in the stiffness of the equipment table. The horizontal lines show the constraints imposed on u_c and v_c

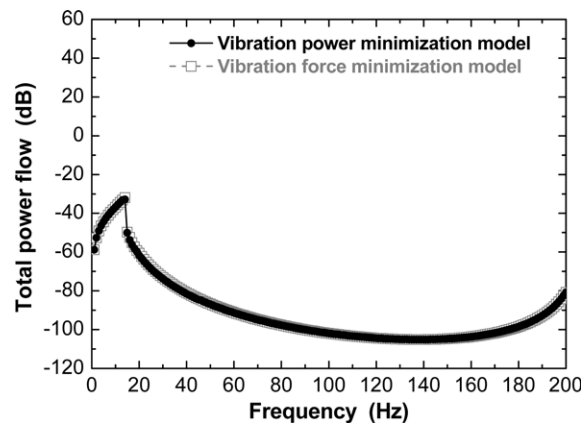


Fig. 7 Frequency dependence of the total power flow to the equipment table obtained from the proposed vibration power minimization model and the conventional vibration force minimization model after an increase of 100 times in the stiffness of the equipment table

Fig. 6, it is found that the proposed vibration power minimization model leads to larger u_c in the 13-60 Hz range (Fig. 6(a)) and v_c in the 13-46 Hz range (Fig. 6(b)). The differences in u_c and v_c at other frequencies are insignificant. No deviations of u_c and v_c from the preset constraints of ≤ 2 mm (Eq. (38)) are observed for the conventional vibration force minimization model.

A similar comparison is plotted in Fig. 7 after an increase of 100 times in the table stiffness. As the first modal frequency of the equipment table is beyond 200 Hz (i.e., at 206 Hz), the equipment table behaves essentially as a rigid support structure in the frequency range of interest. As expected and shown in Fig. 7, the differences in the total power flow to the equipment table obtained by the two vibration minimization models are insignificant for all the frequencies. For such a stiffer equipment table, the design optimization based on the proposed vibration power minimization model provides almost the same results as the conventional vibration force minimization model in

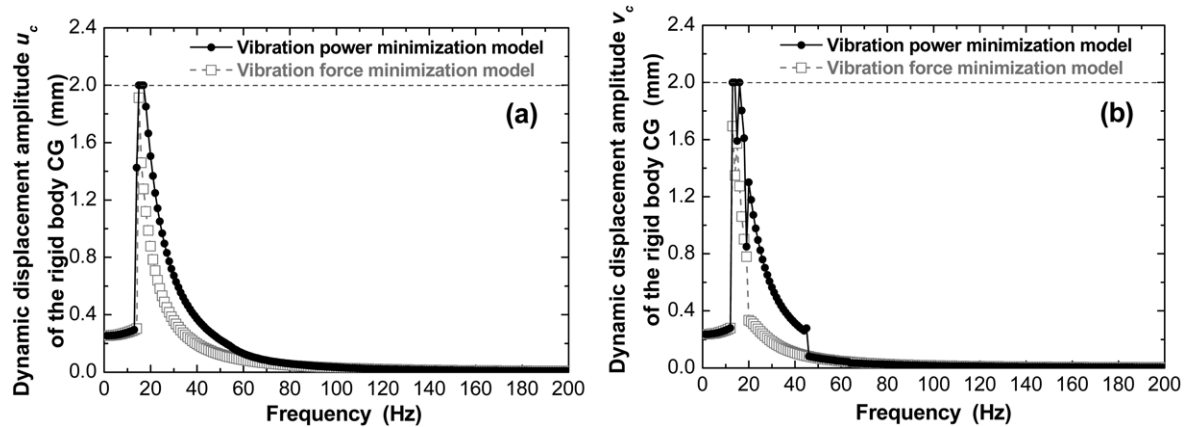


Fig. 8 Comparisons of the dynamic displacement amplitudes (a) u_c and (b) v_c of the CG of the X - Y motion stage obtained from the proposed vibration power minimization model and the conventional vibration force minimization model after an increase of 100 times in the stiffness of the equipment table. The horizontal lines show the constraints imposed on u_c and v_c

term of total power flow. Similar to Fig. 6, the proposed vibration power minimization model still results in larger u_c in the 13-60 Hz range (Fig. 8(a)) and larger v_c in the 13-46 Hz range (Fig. 8(b)). Moreover, neither the proposed nor conventional vibration minimization model causes the deviations of u_c and v_c from the preset constraints (Eq. (38)).

6. Conclusions

A vibration power minimization model suitable for investigation of design optimization of a vibration isolation system formed by a vibrating source, multiple resilient mounts, and an elastic support structure has been developed and applied to semiconductor wire-bonding equipment system composed of an X - Y motion stage, multiple resilient mounts, and an equipment table. The objective of design optimization has been set to minimize the total power flow from the X - Y motion stage to the equipment table through all resilient mounts. The stiffness coefficients of the resilient mounts have been selected as the design variables and imposed with an upper bound and a lower bound. The dynamic displacement amplitudes of the CG of the X - Y motion stage have been constrained as well. The total power flow minimized by the developed vibration power minimization model has been computed at each frequency interval in the concerned frequency range for three different stiffnesses of equipment table. The computed results have been compared with those obtained using a conventional vibration force minimization model. The concluding remarks are as follows:

1. When the equipment table is relatively flexible, the total power flow minimized by the developed vibration power minimization model is much smaller than that minimized using the conventional vibration force minimization model at some critical frequencies due to the effects of elastic dynamic characteristics of the equipment table on the design optimization at these frequencies. The maximum reduction in total power flow of 43 dB is achieved in the developed model compared to the conventional model.

2. When a harder equipment table is used, the effects of elasticity of the equipment table on the design optimization is weakened, as evidenced by a significant reduction in the number of modes of the equipment table presented in the frequency range of interest. As a result, the developed vibration power minimization model generates almost the same predictions on the total power flow as the conventional vibration force minimization model in the concerned frequency range.

Acknowledgements

This work was supported by the Innovation and Technology Fund of the HKSAR Government under Grant UIM/117.

References

- Ahn, Y.K., Song, J.D. and Yang, B.S. (2003), "Optimal design of engine mount using an artificial life algorithm", *J. Sound Vib.*, **261**, 309-328.
- Alkhatiba, R., Nakhaie, J.G. and Golnaraghi, M.F. (2004), "Optimal design of passive linear suspension using genetic algorithm", *J. Sound Vib.*, **275**, 665-691.
- Ashrafiuon, H. (1993), "Design optimization of aircraft engine-mount systems", *J. Vib. Acoust. Trans.*, ASME, **115**, 463-467.
- Brake, M.R. and Wickert, J.A. (2005), "Optimizing vibration isolation of flex circuits in hard disk drives", *J. Vib. Acoust. Trans.*, ASME, **127**, 165-172.
- Choy, P.K. and Wong, C.F. (2004), *Experimental Characterization for an X-Y Motion Stage Mounting Systems*, Technical Report 12156, ASM Assembly Automation Ltd., Hong Kong.
- Cremer, L., Heckl, M. and Ungar, E.E. (1988), *Structure-borne Sound (second edition)*, Springer-Verlag, Berlin.
- Fletcher, R. (1987), *Practical Methods of Optimization*, John Wiley and Sons, New York.
- Gardonio, P., Elliott, S.J. and Pinnington, R.J. (1997), "Active isolation of structural vibrations on a multiple-degree-of-freedom system, Part I: Dynamics of the system", *J. Sound Vib.*, **207**, 61-93.
- Goyder, H.G.D. and White, R.G. (1980), "Vibrational power flow from machines into built-up structures: Part I: Introduction and approximate analyses of beam and plate-like foundations", *J. Sound Vib.*, **68**, 59-75.
- Harris, C.M. (2002), *Shock and Vibration Handbook*, McGraw-Hill, New York.
- Koh, Y.K. and White, R.G. (1996), "Analysis and control of vibrational power transmission to machinery supporting structures subjected to a multi-excitation system, Part I: Driving point mobility matrix of beams and rectangular plates", *J. Sound Vib.*, **196**, 496-493.
- Lee, H.J. and Kim, K.J. (2004), "Multi-dimensional vibration power flow analysis of compressor system mounted in outdoor unit of an air conditioner", *J. Sound Vib.*, **272**, 607-625.
- Leo, D.J. and Inman, D.J. (1999), "A quadratic programming approach to the design of active-passive vibration isolation systems", *J. Sound Vib.*, **220**(5), 807-825.
- Nayfeh, T.A., Emaci, E. and Vakakis, A.F. (1997), "Application of nonlinear localization to the optimization of a vibration isolation system", *AIAA J.*, **35**(8), 1378-1386.
- Pinnington, R.J. (1987), "Vibrational power transmission to a seating of a vibration isolated motor", *J. Sound Vib.*, **118**, 515-530.
- Schittkowski, K. (1985), "NLQPL: A FORTRAN-subroutine solving constrained nonlinear programming problems", *Ann. Oper. Res.*, **5**, 485-500.
- Snyman, J.A., Heuns, P.S. and Vermeulen, P.J. (1995), "Vibration isolation of a mounted engine through optimization", *Mech. Mach. Theory*, **30**, 109-118.
- Soliman, J.I. and Hallam, M.G. (1968), "Vibration isolation between non-rigid machines and non-rigid foundations", *J. Sound Vib.*, **8**, 329-351.

- Swanson, D.A., Wu, H.T. and Ashrafiuon, H. (1993), "Optimization of aircraft engine suspension systems", *J. Aircraft.*, **30**, 979-984.
- Tao, J.S., Liu, G.R. and Lam, K.Y. (2000), "Design optimization of marine engine-mount system", *J. Sound Vib.*, **235**(3), 477-494.
- Yu, Y.H., Peelamedu, S.M., Naganathan, N.G. and Dukkupati, R.V. (2001), "Automotive vehicle engine mounting systems: A survey", *J. Dyn. Syst. -T.*, ASME, **123**, 186-194.